Biomaterials Science

ROYAL SOCIETY OF CHEMISTRY

PAPER

View Article Online
View Journal | View Issue

Cite this: *Biomater. Sci.*, 2024, **12**, 3345

Combining QCM-D with live-cell imaging reveals the impact of serum proteins on the dynamics of fibroblast adhesion on tannic acid-functionalised surfaces†

Agnes Rogala,‡[a] Daria Zaytseva-Zotova,‡[a] Enrique Oreja,[a] Alejandro Barrantes [b] and Hanna Tiainen *[a]

Nanocoatings based on plant polyphenols have been recently suggested as a potent strategy for modification of implant surfaces for enhancing host cell attachment and reducing bacterial colonisation. In this study we aimed to investigate how serum proteins impact the early adhesion dynamics of human gingival fibroblasts onto titanium surfaces coated with tannic acid (TA). Silicate-TA nanocoatings were formed on titanium and pre-conditioned in medium supplemented with 0, 0.1, 1 or 10% FBS for 1 hour. Dynamics of fibroblasts adhesion was studied using quartz crystal microbalance with dissipation (QCM-D). Time-lapse imaging was employed to assess cell area and motility, while immunofluorescence microscopy was used to examine cell morphology and focal adhesion formation. Our results showed that in serum-free medium, fibroblasts demonstrated enhanced and faster adhesion to TA coatings compared to uncoated titanium. Increasing the serum concentration reduced cell adhesion to nanocoatings, resulting in nearly complete inhibition at 10% FBS. This inhibition was not observed for uncoated titanium at 10% FBS, although cell adhesion was delayed and progressed slower compared to serum-free conditions. In addition, 1% FBS dramatically reduced cell adhesion on uncoated titanium. We revealed a positive relationship between changes in dissipation and changes in cell spreading area, and a negative relationship between dissipation and cell motility. In conclusion, our study demonstrated that serum decreases fibroblasts interaction with surfaces coated with TA in a concentration dependent manner. This suggests that controlling serum concentration can be used to regulate or potentially prevent fibroblasts adhesion onto TA-coated titanium surfaces.

Received 2nd February 2024,
Accepted 15th May 2024

DOI: 10.1039/d4bm00184b

rsc.li/biomaterials-science

Introduction

The success of metallic implants in both orthopaedic and dental applications is largely determined by their ability to integrate with bone and soft tissue.[1–3] Despite biocompatibility and robust mechanical properties of implants, achieving soft tissue integration remains challenging due to infections and inflammation resulting from poor wound healing and regeneration.[4,5] Consequently, current studies focus on the initial stages of cell adhesion following implantation, a critical phase during which various cells establish a biological seal between the implant and its surrounding environment. This barrier is essential for preventing microbial invasion and contributes significantly to the implant's long-term survival.[6]

Various strategies are being employed to modify the implant surface properties, such as roughness, morphology and chemical composition, which aim to enhance cellular attachment and thereby improve healing and regeneration processes.[7] More recent approaches have focused on using various biomolecules to form nanocoatings, including ECM proteins, growth factors, peptides, and polysaccharides.[8] Bioactive layers deposited on implant surfaces demonstrated a strong ability to impact the biological response of the surrounding tissues. For example, titanium (Ti) surfaces coated with collagen I have been shown to accelerate initial attachment and growth of both fibroblasts[9,10] and osteoblasts.[11] Similarly, RGD (Arg–Gly–Asp) peptides immobilised on the titanium dental implants enhanced adhesion and proliferation of fibroblasts and epithelial cells.[12] These monofunctional strategies, however, do not address the problem of poor tissue

[a]*Department of Biomaterials, Institute of Clinical Dentistry, University of Oslo, Postboks 1109 Blindern, 0317 Oslo, Norway. E-mail: hanna.tiainen@odont.uio.no*
[b]*Clinical Oral Research Laboratory, Institute of Clinical Dentistry, University of Oslo, Norway*

†Electronic supplementary information (ESI) available. See DOI: https://doi.org/10.1039/d4bm00184b

‡These authors contributed equally to this work.

integration in its full complexity. Developing surfaces functionalised with molecules that possess multifunctional properties, such as enhancing cell adhesion, preventing bacterial colonisation, and reducing tissue inflammation would facilitate better implant integration.

Currently, polyphenols have emerged as new agents that can modulate the functions of biomaterials, contributing to enhanced tissue regeneration.[13,14] Ti surfaces coated with quercitrin have been found to improve implant integration by increasing fibroblasts attachment, improving the mineralisation processes in mesenchymal stem cells, and inhibiting biofilm formation.[15,16] Tannic acid (TA) is also considered as an interesting candidate for biomedical applications due to its biocompatible nature, antibacterial activity, and unique physicochemical properties that enable it to interact with a broad variety of biological macromolecules (*e.g.* proteins and polysaccharides) and materials.[17,18] Studies investigating the interaction between TA deposited on various surfaces and human cells showed that the molecule promoted adhesion, proliferation and morphological changes of different cell types.[19,20] Additionally, TA inhibited biofilm formation by several bacteria species related to the infections associated with bone-anchored implants.[21–23]

Understanding how cells interact with functionalised surfaces is an essential step in the development of biomaterials that enhance implant integration and tissue regeneration. Traditional techniques for studying these interactions like fluorescence microscopy, atomic force microscopy, western blotting, and ELISA, despite numerous advantages often have limitations such as being time-consuming, expensive, and invasive. Additionally, they usually provide limited real-time insights into adhesion and detachment events because of the necessary steps of fixation and permeabilization.[24–26] Overcoming these challenges, quartz crystal microbalance with dissipation monitoring (QCM-D) has emerged as a powerful tool to study cell behaviour on various substrates. This non-invasive, highly sensitive, and label-free technique allows real-time monitoring of events at material surfaces or within thin films.[27] Its application in cell studies, including those on fibroblasts,[28–33] osteoblasts,[34] epithelial cells[35] and stem cells,[36] has enabled the identification of various key events occurring on the surface throughout cell adhesion: (i) initial attachment, (ii) secretion of ECM components, (iii) cell spreading, (iv) focal adhesions formation, and (v) cytoskeletal rearrangements.[37] QCM-D has been effectively used for monitoring cell response to the uncoated surfaces, including bare titanium,[28] and surfaces pre-coated with various ECM and serum proteins, such as collagen,[29] albumin,[30] and fibronectin[33,36] providing an accurate insight into cell–protein–substrate interactions.

Recently, formation of silicate-phenolic networks has been proposed as a method for the controlled continuous deposition of TA on implant surfaces for improved implant-tissue integration.[38,39] However, the biological response of cells and human tissue to such TA surface modifications remains unclear and further characterisation of the obtained nanocoatings is needed. This study was carried out to investigate the relationship between surface properties, protein adsorption, and the behaviour of hGFs on TA-coated titanium surfaces treated with media containing increasing concentration of serum. QCM-D employed in parallel with time-lapse microscopy enabled a comprehensive analysis of initial attachment and cell behaviour on the studied surfaces, while formation of focal adhesions and changes in cell morphology were assessed by fluorescence staining on cells fixed at several time points.

Materials and methods

Materials

Tannic acid (MW = 1071.2 g mol^{-1}, LOT#MKBN9606 V), HEPES (≥99.5%), NaCl (ACS grade, ≥99.0%), sodium metasilicate pentahydrate (Si_{aq}, ≥95.0%), bovine serum albumin (BSA, cold ethanol fraction, pH 5.2, ≥96.0%), Tween® 20, Triton X-100, phosphate buffered saline (PBS), sodium dodecyl sulphate (SDS), Dulbecco's modified Eagle's medium (DMEM), fetal bovine serum (FBS), propidium iodide (PI), 0.02% trypsin–EDTA solution, paraformaldehyde and mouse monoclonal antibody to vinculin (V9131) were purchased from Sigma-Aldrich. The secondary antibody Alexa Fluor™ 488 goat anti-mouse IgG (A11029), Alexa Fluor™ 568 Phalloidin (A12380) and CellTracker™ Green CMFDA dye were supplied by Invitrogen™. DAPI was purchased from Thermo Fisher Scientific. Solution of penicillin–streptomycin (10 000 units per ml of penicillin and 10 g l^{-1} of streptomycin) and GlutaMAX supplement were obtained from Gibco.

Cells and cell culture conditions

Primary normal human gingival fibroblasts (hGFs) purchased from American Type Culture Collection (ATCC, USA) were cultured in DMEM containing low glucose (1 g l^{-1}), sodium bicarbonate (3.7 g l^{-1}) and supplemented with 10% (v/v) heat inactivated FBS, 100 units per ml of penicillin, 0.1 g l^{-1} streptomycin and 2 mM GlutaMAX. The cells were cultured in a humidified incubator with 5% CO_2 at 37 °C.

For cell experiments, a CO_2-independent cell culture medium (test medium) was prepared. The test medium contained low glucose DMEM (1 g l^{-1} glucose), 10 mM HEPES, 5 mM sodium bicarbonate, 100 units per ml of penicillin, 0.1 g l^{-1} streptomycin, and 2 mM GlutaMAX. The test medium supplemented with 0, 0.1, 1 or 10% FBS was used for cell experiments.

Tannic acid coating solutions

Tannic acid (TA) solutions for coating formation were prepared as described previously.[40] Briefly, TA was dissolved at a concentration of 1 mg ml^{-1} in buffer solutions containing 600 mM NaCl, 100 mM HEPES and 80 μM Si_{aq} at either pH = 6.8 or pH = 7.8. The coated surfaces are referred to as TA68 and TA78 depending on the coating solution pH while the uncoated control surfaces are called Ti.

QCM-D monitoring and time-lapse imaging

Cell adherence to Ti sensors with and without TA nanocoatings was monitored in a QCM-D QSense® window module (QWM 401) using a QCM-D QSense® E4 (Biolin Scientific) and Leica SP8 upright confocal laser scanning microscope (CLSM, Leica microsystems, Germany). The QCM-D and CLSM measurements were not performed simultaneously using the same chamber. Note that the actual flow rates were between 100 and 123% of the set pump rate.

Sensors preparation and TA deposition. Ti-coated quartz crystal sensors (QSX 310) were cleaned according to the manufacturer's protocol. Briefly, the sensors were sonicated in 2% (w/v) SDS for 15 min and then in water for 15 min, rinsed with 96% (v/v) ethanol, dried with nitrogen gas, and finally treated with UV-ozone (Novascan PSD-UV4) for 15 min. The sensors were then equilibrated in the corresponding coating buffer at 100 μl min^{-1} for 30 min and then coated with TA solutions at a flow rate of 100 μl min^{-1} for 30 min. The polyphenol solutions were gently stirred (100 rpm) during the coating procedure to provide sufficient oxygen supply. The coated sensors were rinsed in the respective buffer solution at 100 μl min^{-1} for 30 min to remove loosely bound material. All procedures were carried out at 37 °C.

Equilibration in medium. For cell experiments, the prepared sensors were equilibrated at 37 °C in serum-free test medium for 1 h to establish a stable baseline (only uncoated Ti) and after that in a respective test medium at a flow rate of 50 μl min^{-1} for 45–60 min. For modelling of protein corona thickness, the sensors were equilibrated in coating buffer and then coating buffer containing the required concentration of FBS was injected at a flow rate of 100 μl min^{-1} for 1 h; this set of experiments was performed at 21 °C.

Cell injection and monitoring. Prior to cell injection, the hGFs were stained with 1 μM CellTracker™ Green CMFDA dye for 30 min at 37 °C. The labelled cells were collected by trypsinisation, dispersed in the corresponding test medium at a concentration 0.5×10^6 cells per ml and injected into a QCM module at 300 μl min^{-1} (30 s). Cell injection procedure was optimised beforehand to ensure even cell distribution on top of the sensor and reproducibility (Fig. S1†). Measurements were performed at 37 °C under 10 μl min^{-1} flow of test medium, which was supplemented with 0.1 μM PI to visualise dead cells. Changes in frequency (ΔF) and dissipation (ΔD) were continuously monitored at several harmonics (n = 3, 5, 7, 9 and 11) overnight. Time-lapse imaging was performed using the CLSM equipped with an OkoLab Stage system maintaining controlled temperature and humidity conditions, and the images were captured with 15 min intervals with a 10×/0.40 HC PL APO CS objective.

QCM-D modelling

Calculations of layer thicknesses were performed with QTools Software (BiolinScientific, V. 3.1.33). The TA layer thickness was calculated according to Sauerbrey model, while protein adlayer thickness was modelled using an extended Voigt viscoelastic model using the 3rd, 5th, and 7th harmonics. Solutions containing 0.1% and 1% FBS had viscosity = 0.73 mPa s and density = 1 g cm^{-3}, while 10% FBS solutions had viscosity = 0.93 mPa s and density = 1.009 g cm^{-3}.[41] The QCM-D experiments were performed in triplicates for each FBS concentration.

Cell morphology and focal adhesions

To assess changes in cell morphology and formation of focal adhesions, the hGFs were cultured on top of Ti disks.

Deposition of TA on Ti disks and equilibration in medium. Polished Ti disks (Ø 6 mm) were cleaned similarly to the QCM sensors and then autoclaved. The TA nanocoatings were formed in aseptic conditions by incubating the disks first in a corresponding buffer for 30 min and then in 2.5 ml per disk of a TA solution on a rocking platform at 30 rpm for 30 min. The coated disks were washed with buffer for 30 min, serum-free medium for 60 min (only uncoated Ti) and then incubated in the corresponding test medium for 45–60 min.

Cell cultivation on Ti disks. The hGF cells were seeded on top of the disks at a density of 1×10^4 cells per well (200 μl per well, test medium) in a 48-well plate and cultured under static conditions at 37 °C in a CO_2-free incubator for 1, 2, 6 and 24 h.

Modified cell seeding procedure. To test the effects of cell seeding procedure, fibroblasts were seeded on top of the disks coated with TA (pH 6.8) for 4 h. Uncoated Ti disks were used as a control. Cells were added at a density of 1×10^4 cells per well (100 μl per well) in medium containing either 0 or 10% FBS and incubated at 37 °C. After 2 h, FBS concentration was adjusted to 10% by adding 100 μl per well of fresh medium containing 20% or 10% FBS, respectively, and cells were incubated for additional 22 h.

Immunofluorescence staining. At each timepoint, HGFs were rinsed with PBS and fixed in 4% (w/v) PFA for 20 min. Cells were then permeabilised with 0.1% Triton X-100 for 10 min and incubated in blocking buffer (5% BSA in PBS) for 60 min. The samples were then treated with anti-vinculin primary antibody (1 : 100 in 1% BSA/PBS for 60 min), and DAPI (0.1 μg ml^{-1} in PBS for 20 min in the dark). Thereafter, the samples were incubated with secondary antibody goat anti-mouse Alexa Fluor™ 488 (1 : 400 in 1% BSA/PBS for 30 min in the dark) and counter-stained with Alexa Fluor™ 568 Phalloidin (1 : 4000 in 1% BSA/PBS for 30 min in the dark) to visualise cytoskeleton organization. All the steps were performed at room temperature. Images were captured under upright CLSM equipped with 20×/0.50 HCX APO L U–V–I and 63×/0.90 HC APO UVIS CS2 objectives.

Data analyses

Origin® version 2022 (OriginLab Corporation, Northampton, MA, USA) was used to create QCM-D and cell motility plots and to analyse differences between the means for statistical significance using a one-way ANOVA with *post-hoc* Tukey test. Data were expressed as mean ± standard deviation. Pierson's correlation coefficient was computed using Excel (Microsoft

365, WA USA). Differences were considered statistically significant at $p < 0.05$ (*), $p < 0.01$ (**), and $p < 0.001$ (***). Confocal microscope images were analysed by using ImageJ Fiji program (NIH, MD, USA).

Results and discussion

TA nanocoating deposition

In the present study, we combined QCM-D monitoring, time-lapse microscopy and immunocytochemistry to investigate the dynamics of cell adhesion process on tannic acid (TA) coated titanium (Ti) surfaces. TA nanocoatings were formed by 30 minutes deposition of TA under non-oxidising (pH = 6.8) or oxidising (pH = 7.8) conditions in the presence of silicic acid as reported previously.[38,39] The coating process was slower at pH 6.8 (Fig. S2†) and the TA layer reached a thickness of 2.9 ± 0.7 nm (37 °C, $n = 7$). In comparison, deposition of TA at pH 7.8 resulted in a thicker layer of 7.3 ± 1.5 nm (37 °C, $n = 12$). These results correspond well to the previous report showing that initial adsorption kinetics of TA is considerably slower at lower pH.[39] Importantly, the roughness of the tested surfaces was comparable before and after the coating process (Fig. S3†), which was in agreement with our previous observations for 24 h coatings.[40]

Pre-adsorption of proteins

Upon insertion into the body, implants become immediately covered by the proteins from biological fluids, such as blood and interstitial fluids.[42] The composition, type, amount and conformation of the adsorbed protein layer depend on the physicochemical properties of the underlying surface. Subsequently, this layer plays a key role in mediating cell–surface interactions, including cell adhesion, growth and phenotypic behaviour.[42–44] To evaluate the impact of serum protein adlayer on fibroblast adhesion dynamics, we pre-conditioned the test surfaces with growth medium containing fetal bovine serum (FBS). FBS is a complex mixture of biologically active molecules, including proteins, attachment factors, growth factors and hormones. When these biomolecules make contact with an implant surface, they may bind to it, consequently altering interactions between cells and the implant. Although a standard growth medium is usually supplemented with 10% FBS, *in vitro* cell studies can utilise lower serum concentrations or even serum-free media. Therefore, in this study we analysed cell behaviour in growth medium containing four different FBS concentrations: 0, 0.1, 1 and 10%.

Following the introduction of FBS solutions into a QCM-D chamber, we observed a rapid and concentration-dependent decrease in resonance frequency (Fig. S4 and S5†). After the initial drop, a plateau was reached, characterised by a frequency change (ΔF) of less than 1% per minute. As ΔF is associated with the mass deposited on the crystal surface, the recorded change in frequency suggests a rapid initial protein adsorption that slows down as the surface becomes saturated with the proteins. The final plateau level of ΔF depended on the concentration of FBS, with more concentrated solutions resulting in larger shifts in frequency, suggesting a higher mass of adsorbed proteins on the sensor, which is in line with previous report.[45] Furthermore, ΔF was larger on TA-coated surfaces compared to uncoated Ti. This difference can be attributed to the abundance of hydroxyl groups (OH) present in the phenolic groups of TA, which serve as potential multi-point binding sites for proteins.[46]

In addition, we observed an increase in dissipation (ΔD) following the FBS injection. While ΔD was comparable for 0.1% and 1% FBS, a notable increase was observed at 10% FBS. Overall, TA-coated surfaces yielded more dissipative protein layers than uncoated Ti.

Fig. 1 summarises the thickness of the protein adlayer formed after 1 hour of FBS deposition under model conditions. Thickness of the protein layer serves as an indicator of potential conformational changes for the adsorbed proteins, such as deformation, unfolding, or globular transformation during the adsorption process. Additionally, it provides insights into the orientation of proteins within the layer, indicating the direction in which proteins adhere to the surface.[47] As can be seen from Fig. 1, the thickness of the adsorbed protein layer increased with increasing serum concentration and was comparable for both tested TA coatings. The protein adlayer was thicker on TA coatings than on uncoated Ti in 0.1 and 1% FBS ($p < 0.05$) but was not significantly different between the groups in 10% FBS. The increase of protein adlayer thickness due to TA coating agrees with previous findings for ~250 nm TA nanocoatings.[48]

Cell adhesion dynamics monitored by QCM-D and time-lapse imaging

Cell adhesion dynamics on the prepared TA coatings was assessed by combining QCM-D monitoring with time-lapse imaging. Cells were injected simultaneously into two QCM-modules. One module was installed in the QCM-D analyser,

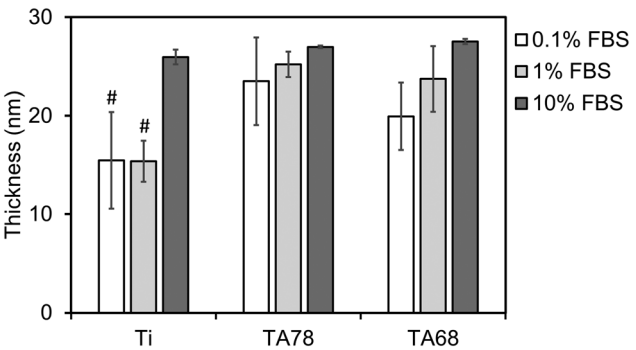

Fig. 1 Thickness of protein adlayer formed on TA-coated (TA68 and TA78) and uncoated titanium surfaces modelled from QCM-D data. The protein adlayer was formed by exposing surfaces to the coating buffer supplemented with 0.1, 1, or 10% FBS during 1 h at a flow rate of 100 µl min^{-1}, 21 °C. The results are presented as mean ± SD ($n = 3–6$). #significantly different from the samples incubated in 10% FBS ($p < 0.01$) and TA78 surface incubated in 0.1 and 1% FBS ($p < 0.05$).

while another module was placed under the confocal microscope. Following cell injection, hGFs were allowed to interact with the sensor surface for approximately 9 h. Longer monitoring was not possible because of air bubbles entering the QCM-D module. To enhance the exchange of nutrients and waste between the cells and their environment, as well as to maintain optimal oxygen concentrations, the fibroblasts were cultured on the examined surfaces under a continuous flow of medium. As no directional motility of the cells was observed, the applied flow rate of 10 μl min^{-1} was considered to have a negligible influence on cell adhesion behaviour, which aligns with previous study.[49] The QCM-D responses for TA68 and TA78 coatings were comparable, hence, only TA78 coatings and uncoated Ti are discussed further in this paper. The QCM-D results are presented for only one representative harmonic (n = 7) since the responses across all harmonics were similar (Fig. S6 and S7†).

Analysis of the QCM-D data (Fig. 2) revealed that hGF cells behaved differently depending on both underlying substrate and amount of the pre-adsorbed serum proteins. The *DF*-plots (Fig. 2A and C) comprised three major phases, each of different duration depending on the protein concentration: phase I lasted for 6–25 min, phase II lasted until 60–500+ min and was followed by phase III. While the QCM-D responses during phase I differed among the tested groups, the *DF*-plots in phase II exhibited similar profiles, characterised by a large shift in dissipation with only minimal changes in frequency. On the contrary, phase III was associated with a large frequency change along with minimal shifts in dissipation. The end of phase II was determined by the time at which ΔD reached a plateau level.

To verify whether the observed shifts in dissipation and frequency for different test conditions were not a result of variations in cell count, we quantified the number of cells present in the QCM-D chamber following cell injection (Table 1). Indeed, comparable number of cells was found on TA-coated surfaces irrespective of FBS concentration. For uncoated Ti and 1% FBS, the cell number on the surface was almost double compared to 0 and 10% FBS.

Cell adhesion to surfaces in the absence of serum is a well-known phenomenon explained by rapid formation of initial connections between cells and surfaces through biomolecules,

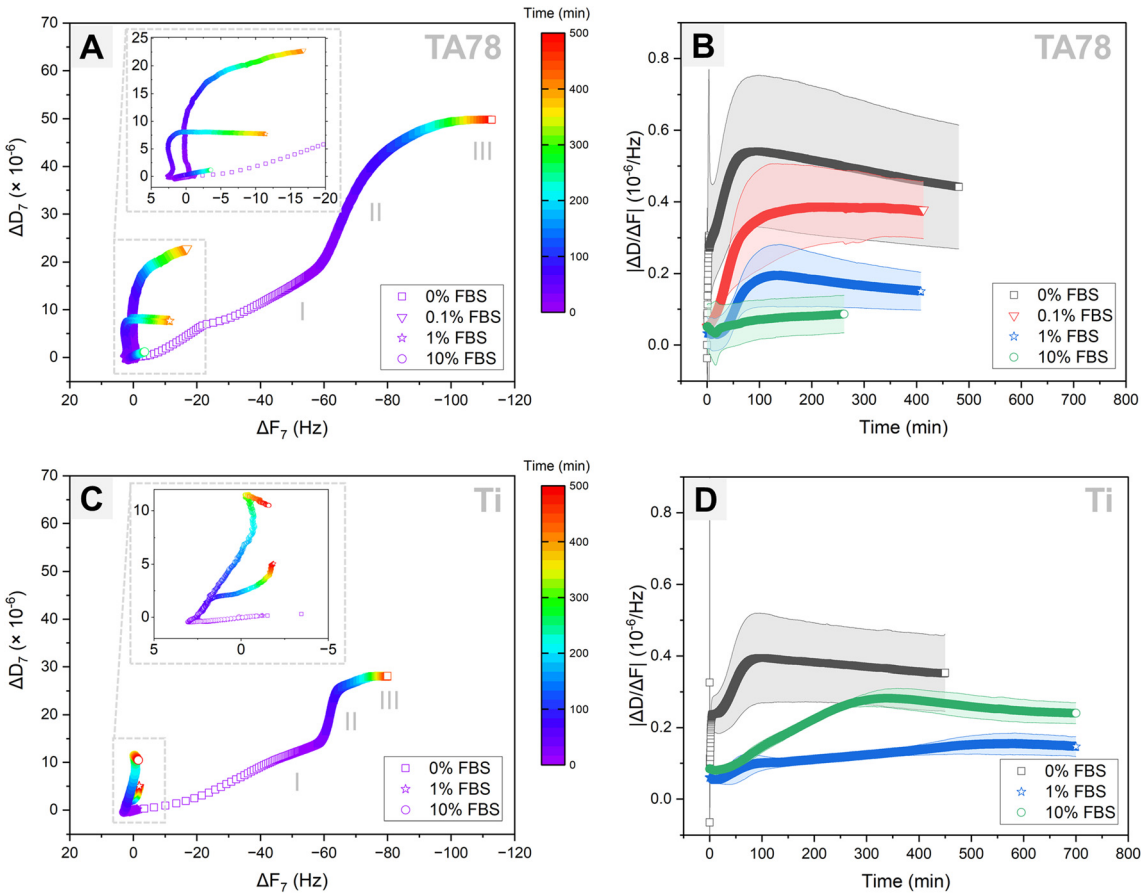

Fig. 2 Averaged *DF*-plots (A and C) and the corresponding $\Delta D/\Delta F$ plots (B and D) for 7th QCM-D harmonic of hGFs adhesion on TA78-coated (A and B) and uncoated (C and D) titanium surfaces pre-conditioned with medium containing 0% (□), 0.1% (▽), 1% (☆), or 10% FBS (○). The insert plots in (A) and (C) are magnified views of the *DF*-plots corresponding to FBS-containing media. I, II, III – major phases of cell–surface interaction. $\Delta D/\Delta F$ was calculated from the dissipation and frequency shifts normalised to the time of growth medium injection, rather than the time of cell injection, to prevent dividing by zero. Mean ± SD (n = 3).

Table 1 Characteristics of cells cultured on top of TA78-coated and uncoated titanium sensors in medium with 0, 0.1, 1 and 10% FBS in a QCM-D module. Total of 65 time-lapse frames were acquired under the confocal microscope, a filmed area was 1.228 mm^2. Mean ± SD (N = 4–8)

Surface	% FBS	Number of cells per filmed area		Viability (%)
		Frame 1	Frame 4	Frame 65[a]
TA78	0	307 ± 10		98.7 ± 0.4
	0.1	265 ± 51		99.2 ± 0.3
	1	371 ± 12		99.4 ± 0.3
	10	348 ± 49[b]	328 ± 44	98.7 ± 0.5
Ti	0	232 ± 55		97.8 ± 1.0
	1	515 ± 60		99.0 ± 0.2
	10	222 ± 66[b]	190 ± 43	97.9 ± 1.2

[a] If an air bubble was observed in the chamber, an earlier timeframe was used to calculate cell viability. [b] Cells did not attach immediately to the surface.

such as cellular fibronectin, and by secretion of fibronectin onto the surface mediating the subsequent cell adhesion and spreading.[50] Following injection of hGFs in serum-free medium, cells promptly sedimented and initiated first interactions (Fig. 3, Video S1†) on TA78 coatings. Fibroblasts generated an abrupt decrease in frequency with accompanying increase in dissipation within the first 4 min (Fig. 2A). This also caused an immediate change in $\Delta D/\Delta F$ (Fig. 2B). Both frequency and dissipation continued to change up to 17 minutes. Notably, for the uncoated titanium, phase I exhibited the same duration and frequency shift (Fig. 2C). This suggested a comparable number of cells (mass) interacting with the surface, indicating that the mass changes near the sensor surface might result from immediate cell adsorption to the surface, followed by cell attachment. However, the overall lower ΔD observed on uncoated Ti during phase I may indicate formation of fewer cell–surface connections compared to TA coatings.

During phase II, the *DF*-plot showed a steep slope, which slowly decreased until dissipation reached a plateau at ~280 minutes (Fig. 2A). At this phase, cells formed multiple protrusions and most of them were spread within ~80 min post-seeding ($\Delta D/\Delta F$ peak). The cells continued to reshape until they occupied maximal area at ~280 min. The observed changes in dissipation can be related to an increase in the degree of formed receptor-mediated cell adhesions,[28,33] increase in cell spreading area, as well as secretion of proteins and other ECM components.[28,31,33,51]

As time progressed, cells acquired more elongated fibroblast-like shape (phase III). This phase, characterized by slowly decreasing ΔF with minimal changes in ΔD, may correspond to ECM remodelling.[28,33]

On the uncoated Ti surface (Fig. 2C), cells exhibited reduced spreading and a higher tendency to cluster compared to TA coatings. Despite similar durations, phases II and III showed lower overall ΔD and ΔF values, indicating a stronger interaction of fibroblasts with TA-coated surfaces in serum-free medium. This effect could be attributed to the natural ability of multiple galloyl groups present in TA to form complexes with proteins, including various integrin ligands.[52] Hence, modification of surfaces with TA can provide more potential adhesion sites for the cells if the protein (integrin ligand) is bound to the substrate in suitable orientation and conformation.

Exposure to a serum-containing medium led to a dramatic change in cell behaviour, indicating that serum proteins pre-adsorbed on TA coatings altered cell adhesion process (Fig. 2A and 3, Videos S2–S4†). In medium with 0.1% FBS, cells rapidly attached to the surface, and started to form first protrusions. This observation can explain the recorded frequency decrease with accompanying dissipation increase during phase I. In the presence of 1% FBS, cells remained spherical for a longer time, but no floating cells were observed, suggesting a delayed cell attachment process. This observation was supported by the QCM-D results, showing only negligible shift in dissipation during this initial phase (phase I). As the serum concentration increased to 10%, cells floated over the surface for about 30 minutes before settling down and initiating attachment.

During the subsequent cultivation period, cells initiated the formation of protrusions on the surfaces and began to spread. In 0.1% FBS, majority of the cells had flattened and adopted a shape similar to those cultured in 0% FBS at ~120 minutes ($\Delta D/\Delta F$ peak) and the cell morphology remained unchanged during phase III. In contrast, 1% and 10% FBS markedly delayed both cell adhesion and spreading, triggering increased cell motility and clustering. In 1% FBS the majority of cells had spread out by the end of phase II. Although cells continued to spread out and flatten over time (phase III), they did not develop a morphology similar to that observed for 0 and 0.1% FBS. In 10% FBS, cell spreading was greatly hindered: only few cells displayed an elongated shape, while the majority remained spherical with limited adhesion points and protrusions.

Increasing the serum concentration in the culture medium from 0.1 to 10% led to a reduction in QCM-D signals. This observation corresponded to a slower and less extensive cell adhesion, with 10% FBS almost completely inhibiting the adhesion process. The hindrance of cell attachment by serum proteins has been previously reported and can be attributed to several factors, including blocking of the surface with proteins that do not contain cell adhesion motifs, *e.g.* albumin.[50] It is important to note that the reduction in QCM-D signals in the presence of serum, may also be related to the thickness of the deposited protein layer, which can potentially reduce the detection depth.[51] However, the profiles of the ΔD *versus* time (Fig. S6†) and $\Delta D/\Delta F$ *versus* time curves (Fig. 2B) support the conclusion of serum concentration-dependent hindrance of cell adhesion: the slope of the curves decreased with an increase in serum concentration.

Similar to TA78 coatings, supplementing the growth medium with FBS induced a delay in the initial cell attachment to uncoated Ti (Fig. 3, Videos S5–S7†). In 10% FBS, cells

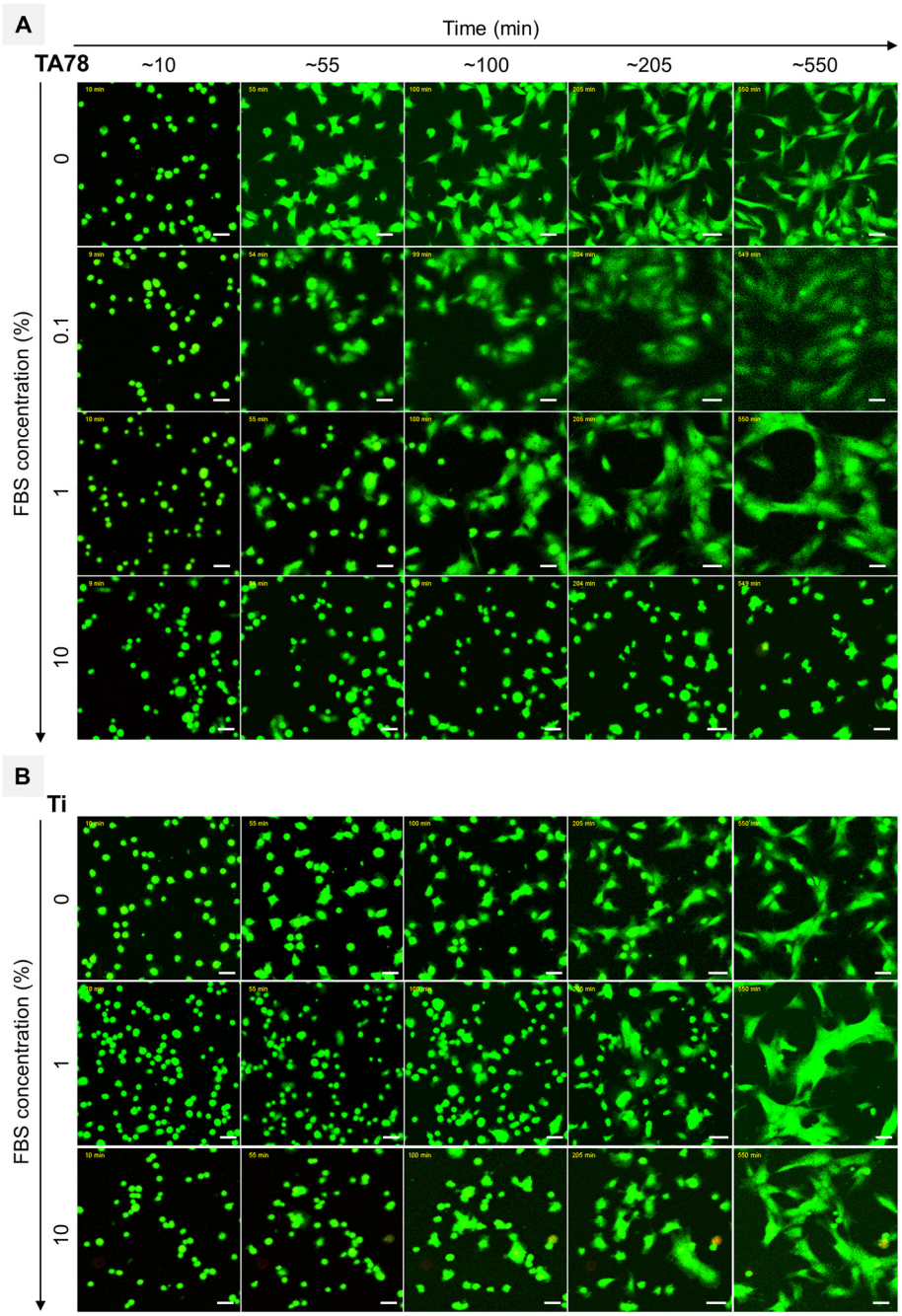

Fig. 3 Time-lapse sequential images showing cell behaviour on (A) TA78 coatings and (B) uncoated titanium in medium with 0–10% FBS. Cells were stained with CellTracker™ Green CMFDA dye (green), dead cells were labelled with PI (red). The results from one representative experiment. Scale bar: 50 μm.

remained mostly spherical and started to change their morphology after ~60 minutes, whereas in 1% FBS cell adhesion was even more delayed, and cells began to elongate and flatten after ~300 minutes. These differences were reflected in *DF*-plots (Fig. 2C). The initial slopes of *DF*-curves were similar for both conditions. However, a change in slope for 1% FBS occurred after ~90 minutes. This indicated that while cell adhesion process continued in 10% FBS, the initial cell attachment was completed in 1% FBS. Fibroblasts spread out and acquired an elongated morphology after ~200 minutes in 10% FBS and ~500 min in 1% FBS. Overall, in 1% FBS, cell adhesion was slower, cells were more motile and tended to cluster more than in 10% FBS. In contrast to TA78-coated surfaces, cell adhesion to uncoated Ti was not directly related to the FBS concentration. Furthermore, several differences were found between uncoated Ti and TA78 coatings, including less steep *DF*-curves slopes, prolonged phase II, and a higher tendency for cell clustering on uncoated Ti. Finally, a total dissi-

pation shift in 1% FBS was lower on uncoated Ti than on TA78 coating, with the opposite trend found in 10% FBS. The results for 10% FBS were consistent with a previous report for hGFs cultured on uncoated Ti in medium with 10% FBS.[28]

$\Delta D/\Delta F$, also known as acoustic ratio, describes the energy loss per unit of the deposited mass. This parameter may be valuable in understanding morphological and cytoskeletal changes in cells, along with receptor–ligand interactions, including the formation and maturation of focal adhesion complexes.[31,33,51] The $\Delta D/\Delta F$ *versus* time curves displayed three major stages: a lag, an increase, and a stationary stage (Fig. 2B and D). In addition to these stages, an instant increase in $\Delta D/\Delta F$ immediately after cell injection was noted in serum-free medium on both surfaces. The lag stage was observed in the presence of serum as well as on uncoated Ti and might indicate a delay in cell adhesion, a phenomenon previously reported on various substrates and linked to the presence of a protein adlayer.[31,53,54] The $\Delta D/\Delta F$ values (Fig. 2B) and the slopes (Table S1†) decreased with increasing serum concentration from 0.1 to 10% on TA78 surface. Furthermore, in serum-free medium $\Delta D/\Delta F$ value and the slope were higher on TA78 than on uncoated Ti probably indicating an enhanced adhesion of fibroblasts on TA-coated surfaces. The opposite was found in 10% FBS.

The timepoint at which the $\Delta D/\Delta F$ curves reached a stationary stage did not necessarily correspond neither to the end of phase II nor the end of cell adhesion process. At this stage we observed an increase in ΔF, while ΔD still continued to increase, though at slower rate. The increase in ΔF might be due to deposition of ECM proteins by the cells, changes in contact area between cells and a surface,[54–56] as well as changes in cell mechanical properties as a result of cytoskeletal changes leading to changes in energy dissipation.[31,57]

Cell spreading area

Next, we investigated changes in cell coverage over time (Fig. 4) as this is an important indicator of cell interaction with the surface. Changes in cell area on the TA78 coatings over time are presented in Fig. 4A. HGFs attached and started to spread at early stages of the experiment, as can be also seen in Fig. 3. The cell area reached its maximum at 2–4 hours, and then began to gradually decline. This decrease in area could be attributed to increased cell motility and clustering at later time points for 1% FBS. For other conditions it could be a result of underestimation of cell area due to cell flattening, as explained below. The cells cultured in 0.1% FBS exhibited the largest spreading area indicating the highest degree of cell adhesion. On the contrary, cells cultivated in 10% FBS exhibited the smallest spreading area, suggesting relatively weak cellular adhesion and spreading.

For uncoated Ti (Fig. 4B), the process of cell adhesion and spreading required a longer time compared to TA coatings, and the extent of cell spreading was notably reduced, which corresponds well to the QCM-D data. Cells cultured in 1% FBS exhibited notably limited surface coverage. In 10% FBS, cells initially spread slower than in serum-free conditions, yet they reached a similar maximum spread area after ~300 minutes. This behaviour differed from that on TA-coated surfaces, suggesting that cells cultured on uncoated Ti in the presence of 10% FBS required time to adapt and remodel the protein layer to establish stable adhesion sites.

While earlier studies have established a linear relationship between cell–surface coverage and resonance frequency change,[54,55] our current findings revealed a different pattern. Specifically, we found no correlation between cell area and ΔF-response (Fig. 4G–J), but we observed a strong linear relationship with ΔD-response (Fig. 4C–F). In the independent analysis of each condition, the Pearson correlation coefficient (r) was $\geq$0.98 ($p < 0.0001$) for 0, 0.1 and 1% FBS and 0.71 ($p < 0.001$) in case of 10% FBS. A low correlation observed for 10% FBS can be explained by an overestimation of cell–surface contact area, which results from the limited interaction of cells with TA surface. However, when we pooled all conditions for analysis, we found no significant correlation ($r = 0.42$) between ΔD and cell area. Similarly, for the uncoated Ti, strong correlation $r \geq 0.95$ ($p < 0.0001$) was found for 0–10% FBS when conditions were examined individually. However, no such correlation was obtained when analysing the pooled data ($r = 0.28$) (Fig. S8†). These findings differ from previous reports showing the linear relationship between dissipation change and percent cell coverage for surfaces coated with various proteins (serum, fibronectin, albumin).[31] Our results showed that the absolute values of ΔD did not reflect differences in cell adhesion rate and the extent of cell adhesion observed for different conditions, although ΔD curves allowed to predict dynamics of cell adhesion.

Although quantification of area from the time-lapse images allowed us to determine the dynamics of cell spreading and compare these results with the QCM-D data, the method has several limitations. First, the initial cell–surface contact area is most likely overestimated since it is impossible to observe contact area formed underneath non-spread spherical cells. Second, at later time points it is difficult to correctly estimate cell area because the fluorescent signal from cell edges becomes weak when cells spread and flatten. Third, the area occupied by individual cells can also be underestimated due to cell clustering and aggregation.

Cell adhesion is a complex dynamic process that involves formation of focal adhesion complexes between the cells and the underlying substrate. The quantity and dynamics of these adhesions greatly depend on various surface parameters. These include the density and availability of cell binding ligands, the rheology and dynamics of the protein adlayer, and the properties of the underlying material. Hence, cells occupying the same area but growing on different substrates may not exhibit the same number and dynamics of focal adhesions. Moreover, cytoskeletal structures and rheology of cells may be different. These changes in cell adhesion behaviour may be reflected in the QCM-D signal as it has been shown that mechanical strength of cell adhesions correlates with a magnitude of the ΔD response.[58] Therefore, a more detailed analysis of changes in cell morphology, focal adhesion formation and

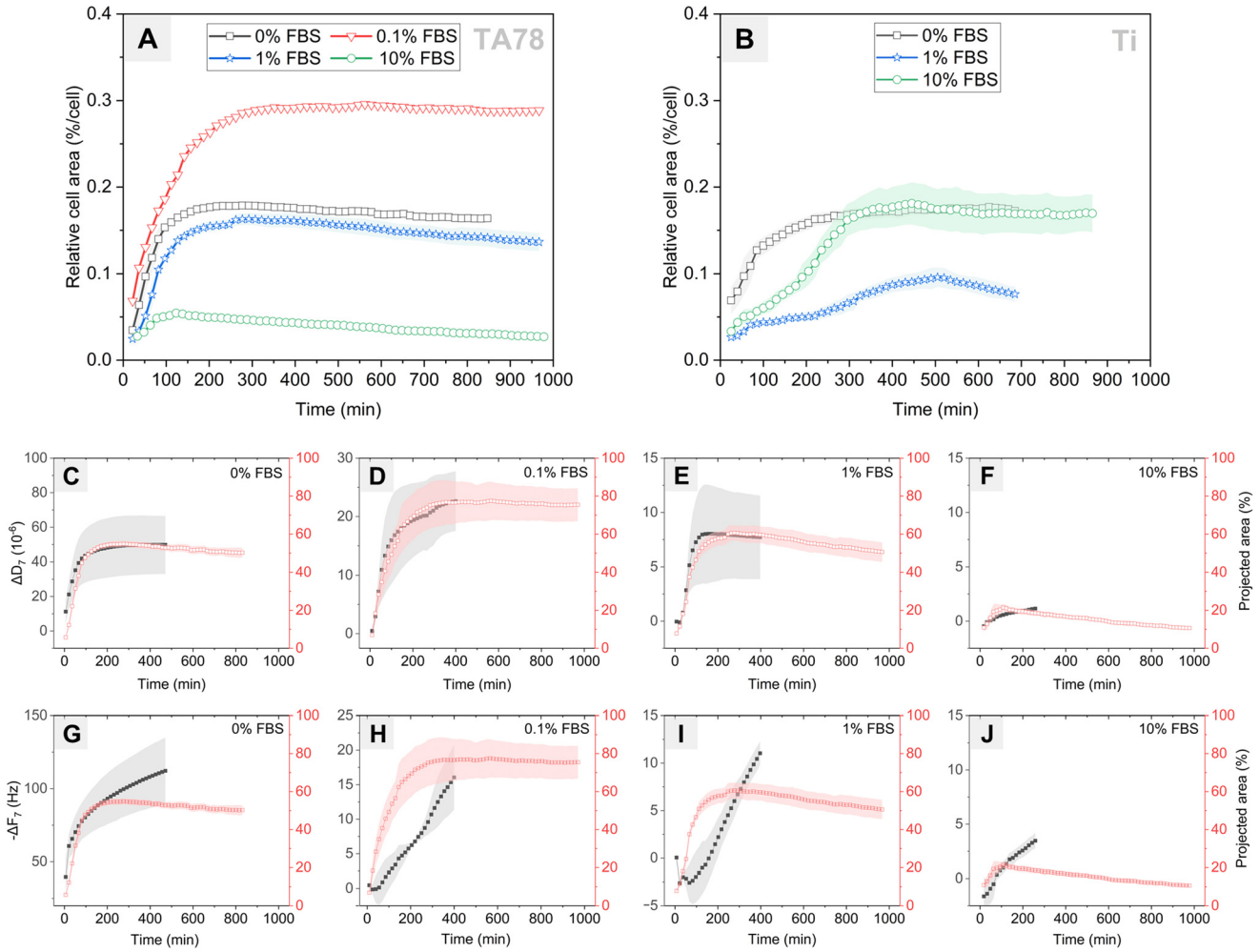

Fig. 4 Adhesion of fibroblasts to TA78-coated (A) and uncoated (B) titanium surfaces in various cell culture media. Plots C–F show the correlation of cell spreading area with averaged dissipation (harmonic 7), while panels G–J demonstrate the correlation with averaged frequency (harmonic 7) on TA78 coating. Relative cell area was calculated as total area occupied by the cells divided by total number of cells on the surface. Each plot shows results from one representative experiment. (C–J) Empty red rectangles represent projected cell area, while black rectangles represent ΔD (C–F) or $-\Delta F$ (G–J). Values are presented as mean ± SD.

cell motility, was conducted next to elucidate the differences between the test conditions observed when using QCM-D.

Cell morphology

To examine cell morphology, we used F-actin staining for cytoskeleton visualisation and vinculin staining to assess focal adhesion formation, a key factor in adhesion strength.

On TA-coated surfaces, a progressive delay in cell attachment, spreading, and focal adhesion formation over time was observed with increasing serum concentrations (Fig. 5A, Fig. S9†). In the absence of serum, we observed an immediate cell adhesion, suggesting that the underlying surface facilitated initial interactions between the cells and the TA nanocoating. Within the first hour post-seeding, cells displayed numerous, thin, and long protrusions extending radially from the periphery. Focal adhesions started to form within 2 h, signifying the initiation of robust cellular anchoring. As the cell culture progressed, fibroblasts manifested an extensive actin network enriched with thick stress fibres, indicating a well-organised cytoskeleton. Elongated and well-defined focal points were co-aligned with stress fibres and oriented along the major cell axis. This robust cellular morphology remained well-preserved throughout the 24-hour cultivation period.

The initial dynamics of cell attachment and spreading in the presence of 0.1% FBS was slightly slower than in serum-free medium. During early timepoints, fibroblasts displayed reduced spreading, characterized by an irregular morphology and fewer filopodia. However, an improved cell spreading was observed over time. Ultimately, the cells acquired elongated shape and exhibited the largest spreading area among all examined conditions. FA formation was first observed as early as 2 h post-seeding, with the complexes primarily localised at the periphery of the cells. By the 24 h timepoint, majority of the cells exhibited visible FAs, indicating robust cell attachment.

Increasing the serum concentration to 1% resulted in a notable delay in both cell attachment and spreading, that was

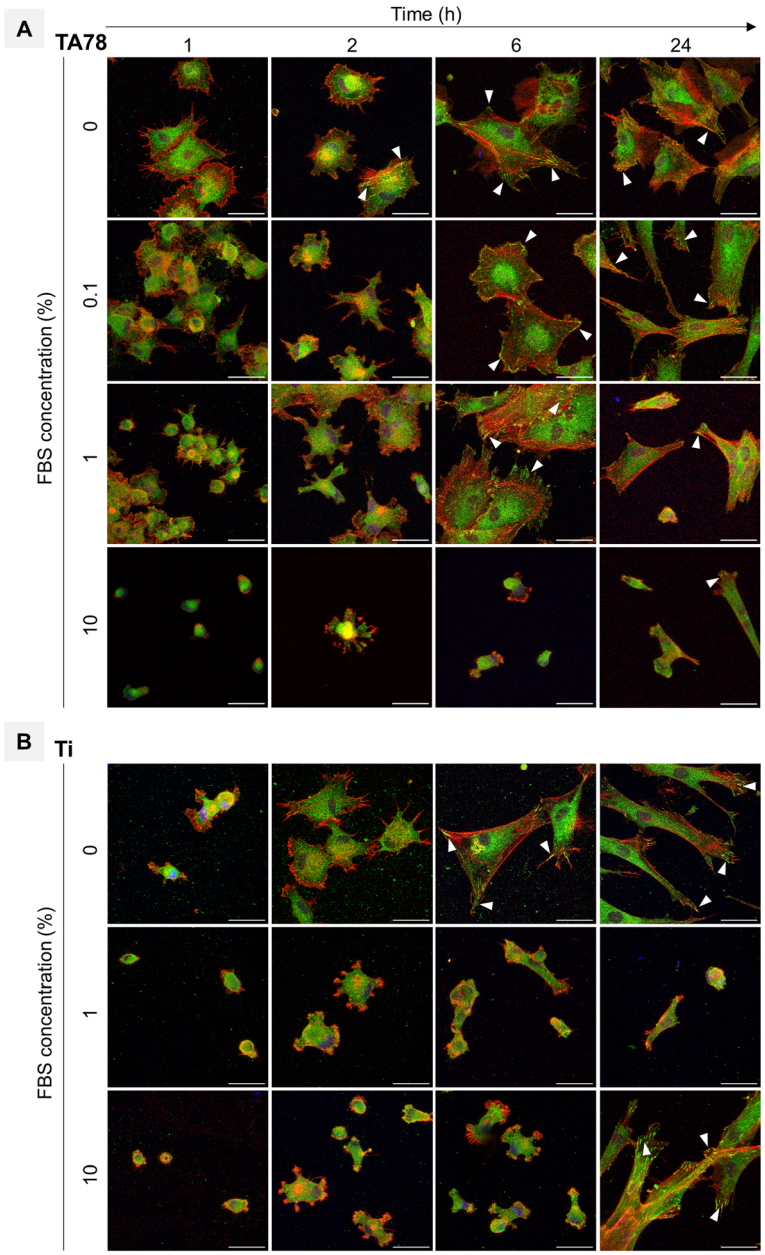

Fig. 5 Representative fluorescence microscopy images of hGF cells cultured on TA78-coated (A) and uncoated (B) titanium disks. The cells were grown in culture medium supplemented with 0, 0.1, 1 or 10% FBS for 1, 2, 6 or 24 hours. Immunostaining of actin (red), vinculin (green) and nuclear DNA (blue). Scale bar: 40 μm.

accompanied by cell aggregation. Initially, the fibroblasts adopted a morphology similar to those cultured in 0.1% FBS. At the 6 h timepoint, the cells had spread out and formed robust focal adhesion points. After 24 h of culture, mainly cell clusters with few focal adhesions were observed.

Supplementation of culture medium with 10% FBS resulted in a significant reduction in the number of attached cells. The cells adopted a rounded morphology with limited spreading, and formed wide, actin-rich lamellipodia typical for migrating cells exploring the underlying substrate. Furthermore, focal adhesion formation was dramatically altered, with only few adhesion points observed by the end of experiment.

On uncoated Ti, cell adhesion and spreading were slightly delayed compared to TA (Fig. 5B). Within the first hour post-seeding, mainly small fibroblasts with spherical or irregular shapes were observed. In the absence of pre-adsorbed proteins, cells started to spread as early as 1 h post-seeding and formed focal adhesions after 2 h of adhering. By 6 h, majority of the cells had acquired triangular or polygonal shape with numerous focal adhesions. Eventually, cells became elongated and firmly attached to the surface *via* focal adhesions. Fibroblasts cultured in 1 and 10% FBS displayed wide lamellipodia with few focal adhesions during the early stages of cell adhesion (up to 6 h). Cells cultivated in 1% FBS exhibited a

consistently irregular morphology throughout the experiment. In contrast, in 10% FBS cells eventually spread acquiring elongated shape with numerous focal adhesions localised mainly at cell peripheries. And after 24 h, noticeably more focal adhesions were observed in fibroblasts cultured in 10% FBS compared to those in 0% FBS.

Fibroblasts grown on uncoated Ti in 0 or 10% FBS, as well as on TA coating in 0 or 1% FBS, achieved a comparable cell area (Fig. 4A and B). However, different morphologies and QCM-D responses were observed. This can be due to differences in the nature of the contact between fibroblasts and the underlying substrate. When cells grow in a stationary state, they tend to form a cytoskeleton with abundant actin-rich fibres that terminate at focal contacts. As the area of these contacts increases, cell adhesion strength becomes higher.[59–62] Cells that exhibit strong adhesion to the surfaces can even become immobilised. On the other hand, less developed mesh-like cytoskeleton with reduced number of formed focal contacts will be more characteristic for less adhesive and more motile cell behaviour.[63] Thus, these morphological differences may be reflected in the observed QCM-D signals, as cytoskeletal polymerisation and formation of cell–substrate adhesions influence cell rheology and cell adhesion force, which can be measured by QCM-D.

Cell motility

Upon interaction with the TA surfaces, fibroblasts exhibited adhesive and motile behaviours, which depended on the concentration of serum in culture medium (Fig. 6A–D and H). In the absence of protein adlayer, most cells remained immobile over the course of the experiment. In 0.1% and 1% FBS, fibroblasts exhibited a comparable motility and covered similar distances. The highest cell motility was observed for the cells cultured in 10% FBS, which aligned well with the visualised cell morphology (Fig. 5).

In contrast, on uncoated Ti, the motility of the hGFs did not correlate with serum concentration (Fig. 6E–G and I). Cells cultured in serum-free conditions exhibited minimal motility but travelled longer distances than those cultured in the same conditions on TA78. Cell motility in medium containing 10% FBS was comparable to that on TA, though cell velocity (as indicated by the slope of the distance-time graph, Fig. 6I) increased over time on uncoated Ti and decreased on TA. The highest cell motility was observed in 1% FBS, and cell velocity increased over the cultivation period. The observed differences in cell motility could be attributed to differences in the protein adlayer composition, such as density and availability of cell attachment ligands.[42]

Comparison of the motility results with the data from QCM-D analysis and microscopic observations revealed an inverse relationship between cell motility and several factors: the rate of cell adhesion, cell spreading, formation of focal adhesions as well as the dissipation shift. This aligns with previous research indicating that increased cell motility is often associated with reduced cell–substrate interactions and reduction of focal adhesion establishment.[64] Hence, our motility results indirectly showed that the observed low dissipation shifts in the presence of serum could be due to fewer (or weaker) contacts formed between cells and the substrate. This aligns with previous findings demonstrating a linear relationship between dissipation shift and focal adhesions formation.[58]

Relationship between QCM-D signal and cell–surface interactions

Cell interaction with QCM-D sensor and the obtained F and D responses are typically presented as DF-plots, which are fingerprints of cell adhesion process. Interpretation of these plots, however, remains challenging as cell adhesion is a complex and dynamic process influenced by many factors, including cell type, culture conditions, and underlying substrate. Cell adhesion encompasses several stages, such the initial attachment to the surface, cell activation and formation of contact points with the surface leading to cell spreading, cytoskeleton reorganisation, maturation of focal adhesion points, and secretion of ECM proteins. Since these major stages of cell–surface interaction have been shown to be reflected in the QCM-D responses,[37] we utilized time-lapse imaging to facilitate interpretation of the obtained QCM-D responses in our study.

The initial phase I identified in our QCM-D analysis corresponded to the settling and initial attachment of cells. This phase was characterized by QCM-D responses that were different among various test conditions. In serum-free medium, cells immediately began to interact with the surface, which caused rapid shifts in both dissipation and resonance frequency. Increasing the serum concentration in the medium led to a delay in cell attachment and, consequently, lower dissipation and frequency shifts.

In the subsequent phase II, we observed cell spreading and notable changes in dissipation with only minimal changes in frequency for all test conditions. Cell area was increasing until it reached a maximum at the end of phase II. According to the analysis of cell morphology during this phase, cells underwent marked structural rearrangement of F-actin cytoskeleton and established multiple cell–surface contacts. These changes were accompanied by an increase in acoustic ratio ($\Delta D/\Delta F$), indicating enhanced cell adhesion. In addition, the analysis of cell motility at this phase showed that more motile cells, often exhibiting lower degree of cell adhesion, caused overall lower shifts in both frequency and dissipation.

The final phase III, distinguished primarily by large frequency changes and minimal changes in dissipation, suggests the maturation of cell–surface connections and ECM remodelling, evidenced by the stability of cell area during this period. In the presence of serum, cell clustering and dynamic changes in protein layer additionally contributed to the QCM-D responses at this phase.

Modification of cell seeding procedure

The results of the current study indicated that gingival fibroblasts are not able to attach and spread on TA-coated surfaces

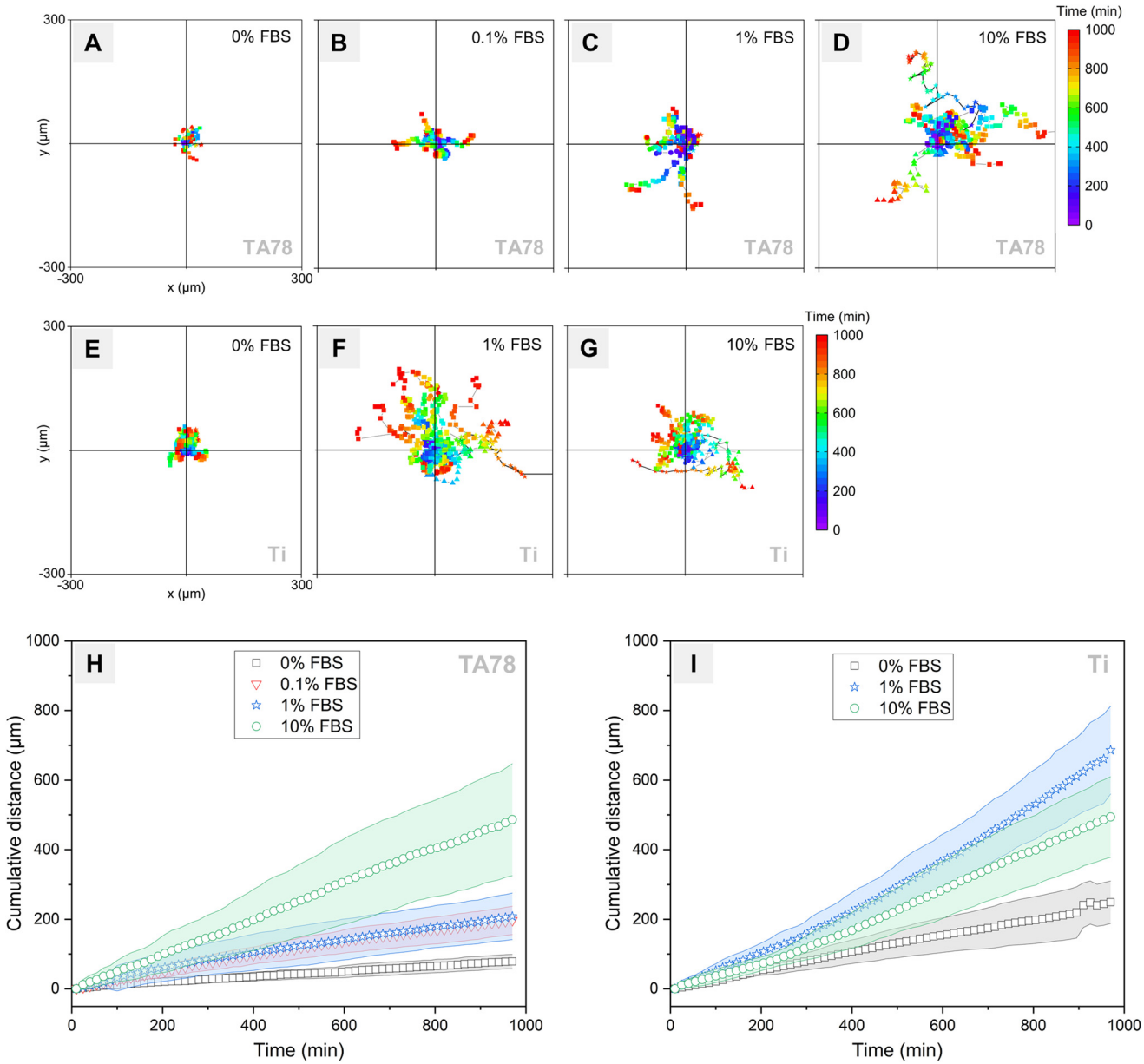

Fig. 6 Effect of FBS concentration in culture medium on HGFs motility on TA78 coated (A–D and H) and uncoated (E–G and I) titanium surfaces. FBS concentration in medium was 0, 0.1, 1 and 10%. (A–G) Each line in the graphs shows the trajectory of an individual cell (n = 10) over 1000 min. The interval between the data points is 15 min. The tracks correspond to one representative time-lapse experiment per tested condition. (H–I) Accumulated distance travelled by the cells over time. Each plot shows results from one representative experiment. Mean ± SD (N = 40).

under standard cell culture conditions, typically involving a growth medium supplemented with 10% FBS. In contrast, it was demonstrated that fibroblasts can immediately adhere and spread out on the TA coatings in serum-free medium. Yet, a long-term cell cultivation in the absence of serum is unsustainable, as it can induce cell starvation and reduce cell viability.

To cultivate cells effectively on TA coatings, a two-stage cell culture method was suggested. First, cells were seeded in a serum-free medium to minimise binding of unwanted proteins and facilitate cell adhesion. Two hours later, as the cells approached their maximum spread area, the medium was switched to one with 10% FBS, providing the nutrients and growth factors essential for long-term cultivation. This approach markedly improved cell adhesion to TA surfaces (Fig. 7). After 24 hours, the fibroblasts exhibited elongated morphology, well-developed F-actin cytoskeleton, and robust focal adhesions (Fig. 7B and C). In contrast, only a small fraction of cells adhered to TA when cells were seeded and cultured in 10% FBS (Fig. 7A). Note that cell behaviour did not change whether the Ti disks were pre-incubated in the medium with 10% FBS for 1 hour or not. Notably, this

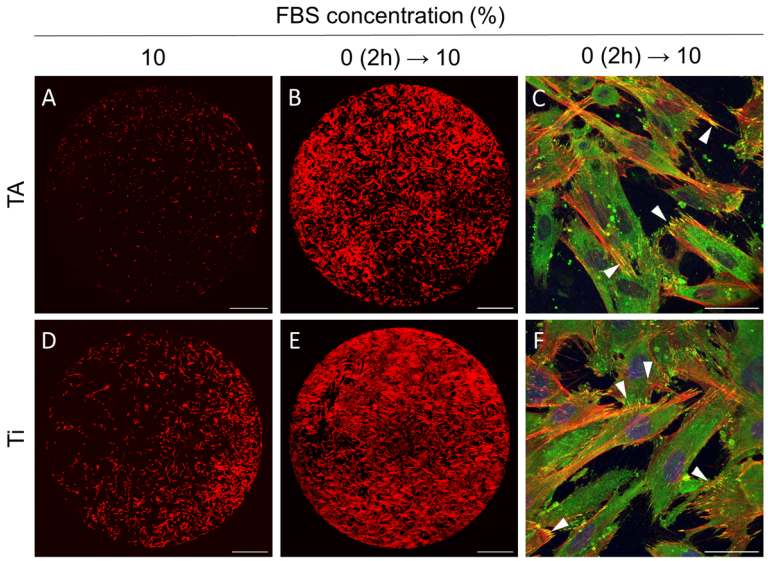

Fig. 7 Effect of cell seeding procedure on fibroblasts morphology and distribution on TA-coated (A–C) and uncoated (D–F) titanium disks. (A and D) Cells were seeded and cultivated in medium containing 10% FBS. (B, C, E and F) Cells were seeded in a medium containing 0% FBS, and after 2 hours, it was changed to a 10% FBS-containing medium. Representative confocal laser scanning microscopy images were acquired after 24 hours of cultivation using (A, B, D and E) a 5× air objective and (C and F) a 63× water objective. The TA coating was deposited on titanium disks at pH 6.8 during 4 hours. F-actin (red), vinculin (green) and nuclear DNA (blue). F-actin colocalised with vinculin at focal adhesion sites, several focal adhesions are indicated by white arrows. Scale bars: 1000 μm at 5× magnification, and 40 μm at 63× magnification.

approach also improved cell adhesion on unmodified Ti surfaces (Fig. 7D–F).

Conclusions

Our study offers an important insight into the initial stages of cell adhesion on both uncoated and TA-coated titanium surfaces, as well as into the impact of serum proteins on cell–substrate interactions. We showed that modification of titanium surfaces with TA could enhance initial adhesion and spreading of gingival fibroblasts and development of focal adhesions. However, this effect was only observed at low concentrations of FBS (0 and 0.1%). Higher FBS concentrations (1 and 10%) resulted in increased fibroblast motility, delayed cell adhesion and altered dynamics of focal adhesions. These findings differed from those on uncoated Ti surfaces and could be attributed to alterations in the serum protein adlayer on TA coatings. The ability of TA-coated surfaces to reduce fibroblasts adhesion in the presence of physiologically relevant serum protein concentrations might be advantageous for applications where limiting fibroblast attachment is crucial to prevent excessive fibrous tissue formation and fibrosis. However, further studies are needed for exploring interactions between serum proteins and TA nanocoatings.

Author contributions

A. R. and D. Z. contributed equally. Conceptualization and supervision: A. B., D. Z., H. T.; Investigation, formal analysis and data curation: A. R., D. Z., E. O.; Writing – original draft: A. R., D. Z., E. O.; Writing – review & editing: all authors.

Conflicts of interest

There are no conflicts to declare.

Acknowledgements

The authors are thankful to Dr Catherine Anne Heyward for helping with confocal microscopy. The study was financially supported by the Research Council of Norway (project no. 302590).

References

1 T. Albrektsson, P. I. Branemark, H. A. Hansson and J. Lindstrom, *Acta Orthop. Scand.*, 1981, **52**, 155–170.
2 S. Bauer, P. Schmuki, K. von der Mark and J. Park, *Prog. Mater. Sci.*, 2013, **58**, 261–326.
3 I. Abrahamsson, T. Berglundh and J. Lindhe, *J. Clin. Periodontol.*, 1997, **24**, 568–572.
4 A. Sculean, R. Gruber and D. D. Bosshardt, *J. Clin. Periodontol.*, 2014, **41**, S6–S22.
5 R. E. Jung, B. E. Pjetursson, R. Glauser, A. Zembic, M. Zwahlen and N. P. Lang, *Clin. Oral Implants Res.*, 2008, **19**, 119–130.

6 T. Q. Guo, K. Gulati, H. Arora, P. P. Han and B. Fournier, *Dent. Mater.*, 2021, **37**, 816–831.
7 E. Rompen, O. Domken, M. Degidi, A. E. F. Pontes and A. Piattelli, *Clin. Oral Implants Res.*, 2006, **17**, 55–67.
8 K. Gotfredsen, in *Implant surfaces and their biological and clinical impact*, Springer, 2015, pp. 147–155.
9 M. Nagai, T. Hayakawa, A. Fukatsu, M. Yamamoto, M. Fukumoto, F. Nagahama, H. Mishima, M. Yoshinari, K. Nemoto and T. Kato, *Dent. Mater. J.*, 2002, **21**, 250–260.
10 N. Marin-Pareja, E. Salvagni, J. Guillem-Marti, C. Aparicio and M. P. Ginebra, *Colloids Surf., B*, 2014, **122**, 601–610.
11 H. Schliephake, A. Aref, D. Scharnweber, S. Bierbaum, S. Roessler and A. Sewing, *Clin. Oral Implants Res.*, 2005, **16**, 563–569.
12 B. H. Zhao, W. M. Tian, H. L. Feng, I. S. Lee and F. Z. Cui, *Curr. Appl. Phys.*, 2005, **5**, 407–410.
13 A. Shavandi, A. E. A. Bekhit, P. Saeedi, Z. Izadifar, A. A. Bekhit and A. Khademhosseini, *Biomaterials*, 2018, **167**, 91–106.
14 J. L. Guo, T. Suma, J. J. Richardson and H. Ejima, *ACS Biomater. Sci. Eng.*, 2019, **5**, 5578–5596.
15 M. Gómez-Florit, M. Monjo and J. M. Ramis, *Sci. Rep.*, 2015, **5**, 16593.
16 M. Gomez-Florit, M. A. Pacha-Olivenza, M. C. Fernández-Calderón, A. Córdoba, M. L. González-Martín, M. Monjo and J. M. Ramis, *Sci. Rep.*, 2016, **6**, 22444.
17 W. Jing, C. Xiaolan, C. Yu, Q. Feng and Y. Haifeng, *Biomed. Pharmacother.*, 2022, **154**, 113561.
18 A. Bigham, V. Rahimkhoei, P. Abasian, M. Delfi, J. Naderi, M. Ghomi, F. D. Moghaddam, T. Waqar, Y. N. Ertas, S. Sharifi, N. Rabiee, S. Ersoy, A. Maleki, E. N. Zare, E. Sharifi, E. Jabbari, P. Makvandi and A. Akbari, *Chem. Eng. J.*, 2022, **432**, 134146.
19 H. Hapidin, N. A. A. Romli and H. Abdullah, *Microsc. Res. Tech.*, 2019, **82**, 1928–1940.
20 X. H. Lv, L. X. Wang, J. J. Fu, Y. Li and L. Yu, *New J. Chem.*, 2020, **44**, 15140–15147.
21 S. Jagani, R. Chelikani and D. S. Kim, *Biofouling*, 2009, **25**, 321–324.
22 V. Sendamangalam, O. K. Choi, D. Kim and Y. Seo, *Biofouling*, 2011, **27**, 13–19.
23 D. E. Payne, N. R. Martin, K. R. Parzych, A. H. Rickard, A. Underwood and B. R. Boles, *Infect. Immun.*, 2013, **81**, 496–504.
24 A. A. Khalili and M. R. Ahmad, *Int. J. Mol. Sci.*, 2015, **16**, 18149–18184.
25 A. Shinde, K. Illath, P. Gupta, P. Shinde, K. T. Lim, M. Nagai and T. S. Santra, *Cells*, 2021, **10**, 577.
26 J. Y. Chen, L. S. Penn and J. Xi, *Biosens. Bioelectron.*, 2018, **99**, 593–602.
27 M. Saitakis and E. Gizeli, *Cell. Mol. Life Sci.*, 2012, **69**, 357–371.
28 E. Westas, L. M. Svanborg, P. Wallin, B. Bauer, M. B. Ericson, A. Wennerberg, K. Mustafa and M. Andersson, *J. Biomed. Mater. Res., Part A*, 2015, **103**, 3139–3147.
29 N. Tymchenko, E. Nileback, M. V. Voinova, J. Gold, B. Kasemo and S. Svedhem, *Biointerphases*, 2012, **7**, 43.
30 M. S. Lord, C. Modin, M. Foss, M. Duch, A. Simmons, F. S. Pedersen, F. Besenbacher and B. K. Milthorpe, *Biomaterials*, 2008, **29**, 2581–2587.
31 M. S. Lord, C. Modin, M. Foss, M. Duch, A. Simmons, F. S. Pedersen, B. K. Milthorpe and F. Besenbacher, *Biomaterials*, 2006, **27**, 4529–4537.
32 W. L. Kao, H. Y. Chang, K. Y. Lin, Y. W. Lee and J. J. Shyue, *J. Phys. Chem. C*, 2017, **121**, 533–541.
33 K. Kushiro, C. H. Lee and M. Takai, *Biomater. Sci.*, 2016, **4**, 989–997.
34 A. Kilic and F. N. Kok, *Biointerphases*, 2018, **13**, 011001.
35 C. M. Marxer, M. C. Coen, T. Greber, U. F. Greber and L. Schlapbach, *Anal. Bioanal. Chem.*, 2003, **377**, 578–586.
36 A. R. Araujo, D. S. da Costa, S. Amorim, R. L. Reis, R. A. Pires and I. Pashkuleva, *ACS Appl. Mater. Interfaces*, 2016, **8**, 28428–28436.
37 C. Fredriksson, S. Kihlman, M. Rodahl and B. Kasemo, *Langmuir*, 1998, **14**, 248–251.
38 F. Weber, A. Barrantes and H. Tiainen, *Langmuir*, 2019, **35**, 3327–3336.
39 F. Weber, W. C. Liao, A. Barrantes, M. Edén and H. Tiainen, *Chem. – Eur. J.*, 2019, **25**, 9870–9874.
40 F. Weber, L. M. Dornelas-Figueira, N. Hafiane, D. Zaytseva-Zotova, A. Barrantes, F. C. Petersen and H. Tiainen, *Colloids Surf., B*, 2022, **219**, 112813.
41 C. Poon, *J. Mech. Behav. Biomed. Mater.*, 2022, **126**, 105024.
42 C. J. Wilson, R. E. Clegg, D. I. Leavesley and M. J. Pearcy, *Tissue Eng.*, 2005, **11**, 1–18.
43 A. Carré and V. Lacarrière, *J. Adhes. Sci. Technol.*, 2010, **24**, 815–830.
44 E. N. Jia, X. Zhao, Y. Lin and Z. H. Su, *Appl. Surf. Sci.*, 2020, **529**, 146986.
45 M. Wilhelmi, C. Müller, C. Ziegler and M. Kopnarski, *Anal. Bioanal. Chem.*, 2011, **400**, 697–701.
46 H. Jafari, P. Ghaffari-Bohlouli, S. V. Niknezhad, A. Abedi, Z. Izadifar, R. Mohammadinejad, R. S. Varma and A. Shavandi, *J. Mater. Chem. B*, 2022, **10**, 5873–5912.
47 M. M. Ouberai, K. Xu and M. E. Welland, *Biomaterials*, 2014, **35**, 6157–6163.
48 F. Weber, H. Q. Quach, M. Reiersen, S. Y. Sarraj, D. N. Bakir, V. A. Jankowski, P. H. Nilsson and H. Tiainen, *J. Biomed. Mater. Res., Part A*, 2022, **110**, 1341–1355.
49 L. Nowacki, J. Follet, M. Vayssade, P. Vigneron, L. Rotellini, F. Cambay, C. Egles and C. Rossi, *Biosens. Bioelectron.*, 2015, **64**, 469–476.
50 F. Grinnell and M. K. Feld, *Cell*, 1979, **17**, 117–129.
51 C. Fredriksson, S. Khilman, B. Kasemo and D. M. Steel, *J. Mater. Sci. Mater. Med.*, 1998, **9**, 785–788.
52 L. Yang, L. Han, Q. Liu, Y. Xu and L. Jia, *Acta Biomater.*, 2017, **64**, 187–199.
53 J. M. Schakenraad, J. Arends, H. J. Busscher, F. Dijk, P. B. van Wachem and C. R. H. Wildevuur, *Biomaterials*, 1989, **10**, 43–50.

54 C. Modin, A. L. Stranne, M. Foss, M. Duch, J. Justesen, J. Chevallier, L. K. Andersen, A. G. Hemmersam, F. S. Pedersen and F. Besenbacher, *Biomaterials*, 2006, **27**, 1346–1354.
55 J. Redepenning, T. K. Schlesinger, E. J. Mechalke, D. A. Puleo and R. Bizios, *Anal. Chem.*, 1993, **65**, 3378–3381.
56 T. Matsuda, A. Kishida, H. Ebato and Y. Okahata, *ASAIO J.*, 1992, **38**, M171–M173.
57 G. Nimeri, C. Fredriksson, H. Elwing, L. Liu, M. Rodahl and B. Kasemo, *Colloids Surf., B*, 1998, **11**, 255–264.
58 J. Y. Chen, A. Shahid, M. P. Garcia, L. S. Penn and J. Xi, *Biosens. Bioelectron.*, 2012, **38**, 375–381.
59 J. L. Tan, J. Tien, D. M. Pirone, D. S. Gray, K. Bhadriraju and C. S. Chen, *Proc. Natl. Acad. Sci. U. S. A.*, 2003, **100**, 1484–1489.
60 N. D. Gallant, K. E. Michael and A. J. García, *Mol. Biol. Cell*, 2005, **16**, 4329–4340.
61 K. A. Beningo, M. Dembo, I. Kaverina, J. V. Small and Y. L. Wang, *J. Cell Biol.*, 2001, **153**, 881–888.
62 N. Q. Balaban, U. S. Schwarz, D. Riveline, P. Goichberg, G. Tzur, I. Sabanay, D. Mahalu, S. Safran, A. Bershadsky, L. Addadi and B. Geiger, *Nat. Cell Biol.*, 2001, **3**, 466–472.
63 P. A. DiMilla, K. Barbee and D. A. Lauffenburger, *Biophys. J.*, 1991, **60**, 15–37.
64 K. Webb, V. Hlady and P. A. Tresco, *J. Biomed. Mater. Res.*, 2000, **49**, 362–368.